2014 IEEE International Conference on Robotics & Automation (ICRA)
Hong Kong Convention and Exhibition Center
May 31 - June 7, 2014. Hong Kong, China

Efficient Force Exertion for Aerial Robotic Manipulation: Exploiting the Thrust–Vectoring Authority of a Tri–TiltRotor UAV

Christos Papachristos[1], Kostas Alexis[2] and Anthony Tzes[3]

***Abstract*— The issue of efficient large force and moment exertion with Unmanned Aerial Vehicles (UAVs) is the subject of this paper. Inspiration is drawn from the vision of UAVs that are capable of autonomously executing industrial activities, or effectively reconfiguring their environment via forceful interaction. Therein, the technical shortcomings of the potential utilization of conventional underactuated UAV platform designs are examined, in terms of operational effectiveness-versus-safety. The innovative implementation of the direct thrust-vectoring authority of tiltrotor UAV types for forceful interaction is proposed, and its associated technical contributions are analyzed. A methodology is developed for controlled forward thrust force and rotating moment exertion, while ensuring safe operation near the hovering attitude pose. A large force-requiring scenario is assembled, consisting of a realistically-sized object laid on solid ground, regarded as a path-hindering obstacle to be forcefully removed by the UAV via pushing manipulation. To this purpose, a high-end autonomous tiltrotor UAV is employed in order to achieve this environment modification task, relying on a properly synthesized control structure.**

I. INTRODUCTION

Unmanned Aerial Vehicles (UAVs) have surpassed their role as aerial observation platforms. As major flight-worthiness issues are efficiently treated [1], numerous novel applications based on environment interaction are being addressed, such as perching [2], grasping and carrying of objects [3–6], cooperative transportation [7] and manipulation [8, 9], and inspection/micro-manipulation via contact [10, 11]. In this work, the concept of an aerial system capable of actively modifying its environment is envisioned, by executing tasks which require the exertion of significant forces and moments in non-vertical directions wherein UAVs are naturally endowed. Such potential tasks are: a) industrial operations such as drilling, cutting and grinding, or b) manipulation of movable objects such as heavy doors or physical obstacles within constrained spaces in rapid deployment and autonomous exploration scenarios. Therein, controlled large pushing or pulling forces are a prerequisite in order to achieve large-scale environment modification.

Within this paper the innovative exploitation of the direct-thrust vectoring capability of a tiltrotor UAV is proposed for addressing such applications. Rotor-tilting is employed in order to generate large forward-thrusting forces, while the aerial system safely regulates its attitude at the horizontal hovering pose. Furthermore, exerted moment control can be achieved via either differential rotor-tilting, or an active 1-Degree of Freedom (DoF) revolute end-effector.

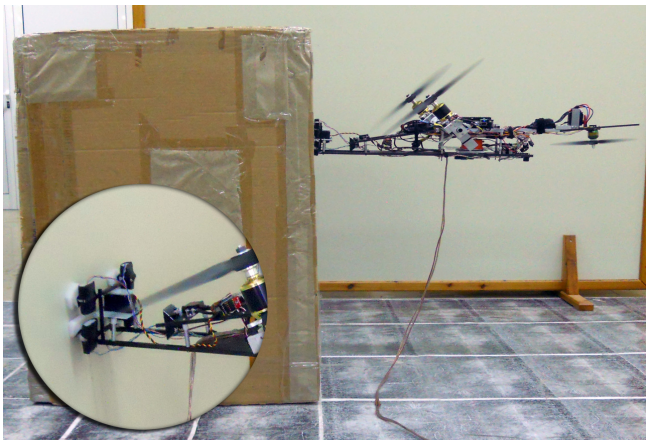

Fig. 1. The UPAT Tri-TiltRotor in Large Force and Moment Exertion, performing Obstacle Manipulation. Detail: The Active End-Effector

The article is structured as follows: In Section II the case-study scenario is analyzed. The system model is presented in Section III and the control synthesis is elaborated in Section IV. Finally, Section V presents the results of experimental studies and Section VI concludes the article.

II. EXPERIMENTAL SETUP

This paper's case-study is illustrated in Figure 2. It consists of the custom-developed [12–14] UPAT Tri-TiltRotor (UPAT-TTR) platform combined with an active 1-DoF revolute end-effector, which is passively compliant and equipped with tactile switches for contact feedback. The full system state estimation is performed on-board the UPAT-TTR, enabling the autonomous execution of the presented scenario.

The environment manipulation objective is the displacement of a free object, along a certain path. This is regarded as a mockup recreation of a rapid indoor deployment scenario, with a heavy obstacle on solid ground [15] constraining the UAV's navigation. In this context the movable object is sized at approximately twice the UAV's own mass, and the inherent ground stiction requires a significant forward-thrusting force to be exerted by the UAV, without risking stability and mechanical/structural safety.

III. SYSTEM MODELING FOR CONTROL

The utilized Body-Fixed Frame (BFF) $\mathbf{B} = \left[B_x,\ B_y,\ B_z\right]$, Object-Fixed Frame (OFF) $\mathbf{O} = \left[O_x,\ O_y,\ O_z\right]$ and North-East-Down (NED) Local Tangential Plane (LTP) $\mathbf{E} = \left[E_x,\ E_y,\ E_z\right]$ are depicted in Figure 2.

[1]C. Papachristos and [3]A. Tzes are with the Electrical and Computer Engineering Department, University of Patras, Eratosthenous 6, Rio 26500, Greece papachric@ece.upatras.gr

[2]K. Alexis is with the Autonomous Systems Lab, Department of Mechanical and Process Engineering, ETH Zurich, Tannenstrasse 3, 8092, Switzerland konstantinos.alexis@mavt.ethz.ch

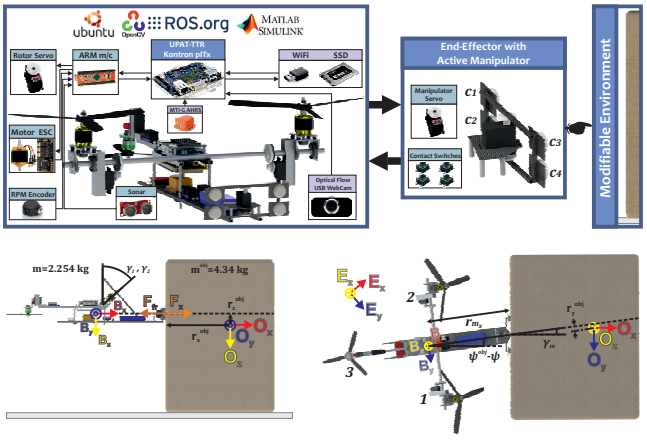

Fig. 2. UPAT–TTR for Exerted Force-Moment Control in an Obstacle Manipulation Study

Let the states $\Theta = [\phi,\ \theta,\ \psi]$ and $\mathbf{X} = [x,\ y,\ z]$ be the LTP-based rotation angles and position vectors respectively. Also, let $i \to \{1,2,3\}$ mark the right, left and tail rotor, $\mathbf{R}_i = [F_i,\ \gamma_i] = [{F^0}_i + \delta F_i,\ {\gamma^0}_i + \delta\gamma_i]$ mark the thrust force and the rotor-tilt angle of the i-th rotor, and γ_m the end-effector angle with respect to the BFF B_x axis. The baseline system state and input vectors used for control are:

$$\mathbf{X} = [\mathbf{X}\ \dot{\mathbf{X}}\ \Theta\ \dot{\Theta}]^T \quad (1)$$

$$\mathbf{U_a} = [\mathbf{R}_1\ \mathbf{R}_2\ \mathbf{R}_3\ \gamma_m]^T\ . \quad (2)$$

Let m and m^{obj} mark the UAV and the object mass respectively, and let $\mathbf{r}_i = [r_{i_x},\ r_{i_y},\ r_{i_z}]$ mark the BFF-based geometric distance from the Center Of Mass (COM) to the i-th rotor's propeller hub, which due to the rotors' hub offsets from their tilt-axes are functions of γ_i [14]. Also, let $\mathbf{r}_m = [r_{m_x},\ r_{m_y},\ r_{m_z}]$ mark the BFF-based geometric distance from the COM to the centroid of the end-effector front plane.

The end-effector front plane centroid can be regarded as a virtual contact point for simplicity, as long as the interfacing contact is normal-to the object surface and $\gamma_m \simeq 0$. This is achieved by actively regulating the UAV attitude at $\{\phi,\ \theta,\ \psi\} \simeq \{0,\ 0,\ \psi^{obj} - \gamma_m\}$, where ψ^{obj} is the LTP-based object orientation. Finally, assuming the aforementioned operational specification and for an object of arbitrary internal structure, let $\mathbf{r^{obj}} = [r_x^{obj},\ r_y^{obj},\ r_z^{obj}]$ mark the OFF-based and γ_m-aligned geometric distance from the virtual contact point to the object's COM, as illustrated in Figure 2.

A. Free–Flight Hovering Mode

In the Free-Flight (FF) mode [12] the control vector $\mathbf{U_{FF}}$ is utilized, and the control allocation $\mathbf{U_{FF}} \to \mathbf{U_a} = \mathbf{U_a^0} + \delta\mathbf{U_a}$ is summarized by:

$$\mathbf{U_{FF}} = [U_x,\ U_y = \phi^r,\ U_z,\ U_\phi,\ U_\theta,\ U_\psi]^T \quad (3)$$

$$\mathbf{U_a} = \begin{bmatrix} {F^0}_1 \\ {\gamma^0}_1 \\ {F^0}_2 \\ {\gamma^0}_2 \\ {F^0}_3 \\ {\gamma^0}_3 \\ {\gamma^0}_m \end{bmatrix} + \begin{bmatrix} \delta F_1 \\ \delta\gamma_1 \\ \delta F_2 \\ \delta\gamma_2 \\ \delta F_3 \\ \delta\gamma_3 \\ \delta\gamma_m \end{bmatrix} = \begin{bmatrix} \frac{c_1\ m\ g}{\cos(U_x)} \\ 0 \\ \frac{c_2\ m\ g}{\cos(U_x)} \\ 0 \\ c_3\ m\ g \\ 0 \\ 0 \end{bmatrix} + \begin{bmatrix} -U_\phi + c_1(U_\theta - U_z) \\ U_x \\ U_\phi + c_2(U_\theta - U_z) \\ U_x \\ c_3(-U_\theta - U_z) \\ -U_\psi \\ 0 \end{bmatrix}, \quad (4)$$

where the r superscript marks the reference value. Forward thrust-vectoring via collective main rotor tilting $\{\gamma_1,\ \gamma_2\} = \gamma_x$ is used for longitudinal control, while the remaining DoFs are handled as in standard tri-rotor configurations. The $\mathbf{U_a^0}$ terms are feedforward-trim values, required in order to retain total vertical force equilibrium. Also c_i are control mixing coefficients guaranteeing moment equilibrium (due to the asymmetrical UAV mechanical configuration). For equally tilted rotors $r_{1_x} = r_{2_x} = r_{1,2_x}$ and thus: $c_1 = c_2 = \frac{r_{3_x}}{2\ (r_{1,2_x} + r_{3_x})}$, $c_3 = \frac{r_{1,2_x}}{r_{1,2_x} + r_{3_x}}$. Finally, in the FF mode the end-effector angle is constantly commanded to $\gamma_m = 0$.

B. Force–Moment Exertion Mode

In the Force-Moment Exertion (FME) mode, the UAV is applying forces onto the docked obstacle via the end-effector interface as visualized in Figure 2. The forward thrusting components of the main rotors are applied longitudinally in the γ_m-direction, provided the stable attitude regulation at $\{\phi,\ \theta,\ \psi\} \simeq \{0,\ 0,\ \psi^{obj} - \gamma_m\}$ is ensured. A friction force F_{fr} appears due to the object-to-ground interface, in the Stribeck [16] generalized form:

$$F_{fr} = \begin{cases} -F_v(u^{obj}), & \text{for } u^{obj} \neq 0 \\ -F_e, & \text{for } u^{obj} = 0 \ \ AND \ \ |F_e| < F_{st} \end{cases}, \quad (5)$$

where u^{obj} the object-to-ground interface relative velocity, F_e the externally applied force, $F_v(u^{obj})$ the viscous friction, and F_{st} the stiction forces. In a realistic scenario, the object's mass, its internal structure and COM placement, and the friction model parameters are uncertain, as even the ground texture can largely vary among areas. The proposed approach for the purposes of this paper is the disjunction of the problem into two separate objectives: a) attitude regulation around the hovering pose while docked, and b) exerted force-moment control for pushing-manipulation.

Concerning the attitude regulation problem, and assuming a forward-exerted pushing force, the UPAT-TTR is considered as attached onto the object surface at the virtual contact point. This is regarded as the new center of rotation, with respect to which the new moments of inertia are recalculated. Additive disturbances on the attitude are mechanically counteracted, as is pointed out in the following analysis. The attitude control allocation principles are similar to [15], wherein collective rotor-thrusting is utilized for pitch θ-regulation. Also in [15], it is noted that during docking with the object no significant disturbing moment is produced onto the UAV, assuming the $\{\phi,\ \theta,\ \psi\} \simeq \{0,\ 0,\ \psi^{obj}\}$ attitude regulation and the mechanical placement of the end-effector's centroid in-line with the vehicle's COM ($\mathbf{r}_m = [r_{m_x},\ 0,\ 0]$), as depicted in Figure2.

Concerning the pushing-manipulation problem, it is assumed that the object COM can move along the O_x-axis and rotate around the O_z-axis. Thus, LTP-based $\{x,\ y\}$ manipulation can be achieved by exerting a forward pushing-force and a rotating moment. Forward thrust-vectoring is employed to generate a controlled longitudinal force, while a rotating moment can be derived via either: a) differential thrust vectoring, or b) active end-effector γ_m control.

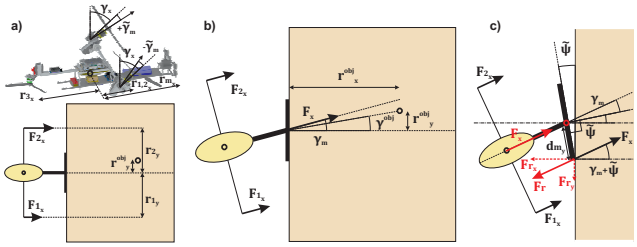

Fig. 3. Rotor-Tilting UAV-based Moment Exertion Principles

These principles are illustrated in Figure 3: In a) the differential thrust-vectoring principle is depicted. Due to the arbitrary internal placement of the object's COM and assuming that the friction forces act on it, in order to control the orientation the UAV must induce a moment $M_z^{obj} \geq 0$:

$$M_z^{obj} = F_{2_x}\ (r_{2_y} - r_y^{obj}) - F_{1_x}\ (r_{1_y} + r_y^{obj}) \geq 0 \quad \Rightarrow \quad \frac{F_{2_x}}{F_{1_x}} \geq \frac{r_{1_y} + r_y^{obj}}{r_{2_y} - r_y^{obj}} \geq 1\ , \tag{6}$$

as $r_{1_y} = r_{2_y}$. In order to achieve $F_{2_x} \geq F_{1_x}$, the rotors are tilted differentially by $\pm\tilde{\gamma}_m$ around a common forward-tilt angle γ_x as in Figure 3-a), and the rotor thrust values are modified to maintain force equilibrium on the vertical axis and moment equilibrium around the roll axis and the new pitch axis (relative to the virtual contact point). For small differential $\tilde{\gamma}_m$, $r_{1_x} = r_{2_x} = r_{1,2_x}$, and near $\{\phi,\ \theta\} = \{0,\ 0\}$:

$$F_1 = \frac{c_1\ m\ g}{\cos(\gamma_x - \tilde{\gamma}_m)}, \qquad F_2 = \frac{c_2\ m\ g}{\cos(\gamma_x + \tilde{\gamma}_m)}, \qquad F_3 = c_3\ m\ g\ , \tag{7}$$

where c_i are the same factors as in the FF mode. It is important to note that this implies differential thrusting of the rotors concurrently to differential tilting, which eventually increases the magnitude of the generated moment, aiding in the UAV's objective. Finally, it is noted that if $r_{2_y} \leq r_y^{obj}$, (6) implies the necessity for negative (pulling) forces.

In Figure 3-b), the active end-effector γ_m control principle is depicted. In order to generate a moment $M_z^{obj} \geq 0$:

$$M_z^{obj} = F_x \sin(\gamma_m) r_x^{obj} - F_x \cos(\gamma_m) r_y^{obj} \geq 0 \quad \Rightarrow \quad \gamma_m \geq \tan^{-1}\left(\frac{r_y^{obj}}{r_x^{obj}}\right) = \gamma_c, \tag{8}$$

the end-effector angle has to become higher than the object COM-to-virtual contact point relative angle γ_c. However γ_m is constrained by the requirement for stable non-sliding contact.

Finally, in Figure 3-c), it is indicated that a counteracting moment appears in the event that during FME the end-effector planar interface is lost. Calculating the total moment with respect to the end-effector centroid for a misalignment error $\tilde{\psi}$ and a reaction force F_r,

$$\begin{aligned} M^m{}_z &= -F_r \sin(\gamma_m + \tilde{\psi})(-d_{m_y} \sin(\tilde{\psi})) - F_r \cos(\gamma_m + \tilde{\psi})(-d_{m_y} \cos(\tilde{\psi})) \\ M^m{}_z &= F_r d_{m_y} \cos(\gamma_m + \tilde{\psi} - \tilde{\psi}) = F_r d_{m_y} \cos(\gamma_m)\ , \end{aligned} \tag{9}$$

which justifies the mechanical design of the end-effector interface (a rectangular frame of $d_{m_y} \neq 0$, instead of a point-edge one), as the resulting moment direction is such that tends to eliminate the misalignment error.

Following the notation of the FF mode, the FME mode control allocation takes the form:

$$\mathbf{U_{FME}} = \left[U_x,\ U_y\ OR\ \tilde{U}_y,\ U_z = 0,\ U_\phi,\ U_\theta,\ U_\psi\right]^T \tag{10}$$

$$\mathbf{U_a} = \begin{bmatrix} F^0{}_1 \\ \gamma^0{}_1 \\ F^0{}_2 \\ \gamma^0{}_2 \\ F^0{}_3 \\ \gamma^0{}_3 \\ \gamma^0{}_m \end{bmatrix} + \begin{bmatrix} \delta F_1 \\ \delta\gamma_1 \\ \delta F_2 \\ \delta\gamma_2 \\ \delta F_3 \\ \delta\gamma_3 \\ \delta\gamma_m \end{bmatrix} = \begin{bmatrix} \frac{c_1\ m\ g}{\cos(U_x - \tilde{U}_y)} \\ 0 \\ \frac{c_2\ m\ g}{\cos(U_x + \tilde{U}_y)} \\ 0 \\ c_3\ m\ g \\ 0 \\ 0 \end{bmatrix} + \begin{bmatrix} -U_\phi + c_1(-U_\theta) \\ U_x - \tilde{U}_y \\ U_\phi + c_2(-U_\theta) \\ U_x + \tilde{U}_y \\ c_3(-U_\theta) \\ -U_\psi \\ U_y \end{bmatrix} \tag{11}$$

where $\mathbf{U_a} = \mathbf{U_a^0} + \delta\mathbf{U_a}$ and the $\mathbf{U_a^0}$ terms marking feedforward values for z-axis and roll-pitch steady-state equilibrium. The z-control is disabled, and the y-control is applied in order to induce a rotating moment via: a) the active end-effector $\gamma_m = U_y$, or b) differential thrust-vectoring $\tilde{\gamma}_m = \tilde{U}_y$.

C. Technical Discussion on Force Exertion via Rotor–Tilting

As discussed, there exists a range of possible tasks which require significant force exertion in non-vertical directions, wherein UAVs are inherently endowed. Such a force can be generated via thrust-vectoring, for which the following two methodologies are possible:

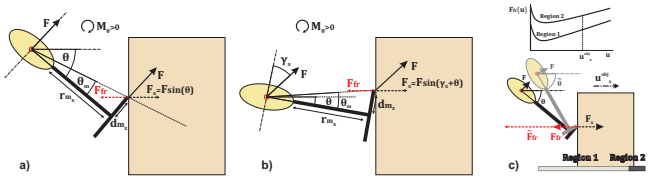

Fig. 4. Technical Analysis of UAV-based Force Exertion Principles

In Figure 4-a), the underactuated dynamics approach is depicted with reference to the object-manipulation case-study scenario for consistency. This practice is elaborated in [17], and is based on the principle of forward-force generation via pitch θ-rotation of the UAV body in order to longitudinally project the total thrust vector. The longitudinally exerted force is $F_x = F\sin(\theta)$, where F the total thrust, commanded as $F = \frac{m\ g}{\cos(\theta)}$ in order to achieve steady-state z-axis and θ moment equilibrium. For a general end-effector design with $d_{m_z} \neq 0$, and assuming there is no vertical sliding motion on the contact interface, moment calculation with respect to the UAV COM yields:

$$F_x = F\sin(\theta) \tag{12}$$

$$M_\theta = (F_{fr} - F_x)\sin(\theta - \theta_m)\sqrt{{d_{m_z}}^2 + {r_{m_x}}^2}\ , \tag{13}$$

where $\theta_m = \tan^{-1}\left(\frac{d_{m_z}}{r_{m_x}}\right)$. When $F_x = F_{fr}$ stiction is in effect, or sliding motion occurs at a certain constant u_x^{obj} as determined by (5). In such cases $M_\theta = 0$. However, for any external disturbance ΔF_{fr}, a disturbing moment will appear, calculated as:

$$\Delta M_\theta \simeq \frac{\partial M_\theta}{\partial F_{fr}}\Delta F_{fr} = (\sin(\theta - \theta_m)\sqrt{{d_{m_z}}^2 + {r_{m_x}}^2})\Delta F_{fr}\ , \tag{14}$$

which for $\theta > \theta_m$ tends to further increase the θ-pitch angle. This effect is intuitively depicted in Figure 4-c, maintaining consistency with a realistic object-manipulation case-study:

the object moves at $u_x^{obj}: F_{fr} = F_v(u_x^{obj}) = F_x = F\sin(\theta)$, while suddenly encountering a drastically different-textured area. Assuming no deformation of the object, a large near-instantaneous ΔF_{fr} appears due to the UAV's velocity near the instant of entering the higher-friction region. This appears as a large disturbing moment onto the UAV COM, leading to a $\Delta\theta$ disturbance. It is noted that the $\theta - \theta_m$ term reduces a potentially destabilizing effect, justifying a rectangular frame end-effector design ($d_{m_z} \neq 0$). However for $\theta < \theta_m$, the F_{fr}-generated moment component is counteracting, implying reduced efficiency.

In order to generate large forward-exerted forces via this (underactuated) approach, the UAV is required to heavily tilt its body. However, for $\theta \gg \theta_m$ the effects of any disturbances on the system's dynamics become more notable as per (14), and the system becomes increasingly reliant on the control authority F in order to handle them. For non-ideal, bandwidth-limited actuation and considering the rigid-body dynamics coupling, the control authority is limited to a certain dynamic and static margin. Eventually, such a system becomes potentially more unstable as an even larger forward-exerted force is required.

In Figure 4-b), the directly-actuated thrust vectoring dynamics approach is illustrated. This practice relies on γ_x rotor-tilting in order to longitudinally project the UAV's propulsion force, while the body pitch is regulated at $\theta \simeq 0$. Here (13),(14) hold for $\theta \gg 0$, while:

$$F_x = F\sin(\gamma_x + \theta) \quad (15)$$

$$M_\theta{}^{\theta\simeq 0} = (F_{fr} - F_x)\sin(\theta) r_{m_x} \quad (16)$$

$$\Delta M_\theta{}^{\theta\simeq 0} \simeq \frac{\partial M_\theta}{\partial F_{fr}} \Delta F_{fr} = (\sin(\theta) r_{m_x}) \Delta F_{fr} \ , \quad (17)$$

where (16),(17) are for $\theta \simeq 0$, as contact forces are assumed to be acting on the end-effector center (the end-effector is planar to the object surface). These indicate the technical achievement accomplished by employing the directly-actuated thrust-vectoring principle: As the forward force component is generated by an additional control authority, the body pitch can be regulated near the hovering attitude pose, which drastically minimizes the effects of any disturbances. Moreover, an end-effector configuration of $\theta_m \neq 0$, generates a counteracting moment while $\theta < \theta_m$, tending to eliminate the disturbing effect of a $\theta_0 \gg 0$ initial condition.

IV. CONTROL SCHEME

The control synthesis illustrated in Figure 5 consists of the Free-Flight and Force-Moment Exertion system modes controllers, and the Finite State Machine (FSM) Supervisory controller. Additionally, the $\mathbf{X_c} = [c_1,\ c_2,\ c_3,\ c_4]$ state vector contains the Boolean (on/off) contact feedback information from the end-effector tactile switches shown in Figure 2, and $\mathbf{X_o} = [x^{obj},\ y^{obj},\ z^{obj}]$ is a reference docking point on the obstacle.

A. Free-Flight Controller

The FF mode control structure is based on gain-scheduled PID-dD (Proportional, Integral, Derivative, double Derivative) output-feedback loops [12]. Feedback gains were obtained via simulated studies on a non-linear mathematical model of the UAV's rotational and translational dynamics. For each DoF a control action of the $\mathbf{U_{FF}}$ vector in (3) is calculated and allocated to the actuation subsystem based on (4). The $\mathbf{U_a^0}$ terms are calculated in a feedforward sense. The attitude-feedback loops operate at $f_\Theta = 100$ Hz, and the translation-feedback loops at $f_X = 10$ Hz.

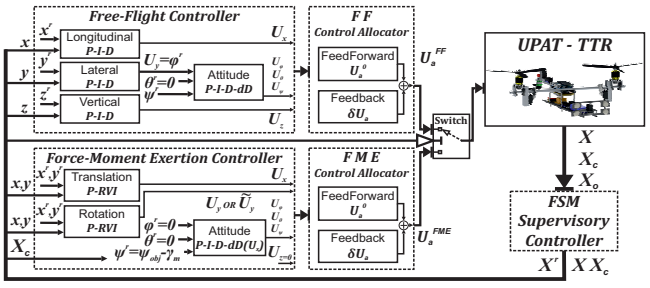

Fig. 5. Control Scheme for Force-Moment Exertion with a Rotor-Tilting UAV in Obstacle Manipulation

B. Force-Moment Exertion Controller

The FME control structure in the object-manipulation case-study assumes one control subsystem for the rotational dynamics in docked-contact, and one for the translational manipulation of the obstacle. As discussed, force exertion via direct rotor-tilting enables constant operation around the planar-contact, hovering-attitude pose $\{\phi,\ \theta,\ \psi\} \simeq \{0,\ 0,\ \psi^{obj} - \gamma_m\}$, where the rotational subsystem dynamics can be considered as decoupled. Thus, an output-feedback control structure similar to the FF one is retained. Stabilizing gains were obtained via simulated studies on the re-evaluated constrained non-linear rotational model (with the rotation axes placed at the virtual contact point). Continuous adaptation of the feedback gains as functions of the rotor-tilt angles γ_i is performed, such that the generated force and moment components controlling each decoupled rotational subsystem remain constant for a given state-error vector. It is noted that the object's orientation ψ^{obj} is not measurable while docked, however the error $e_\psi = \psi - (\psi^{obj} - \gamma_m)$ can be indirectly driven by a logical rule based on the detection of non-bilateral contact as shown in Figure 3-c:

$$e_\psi = \begin{cases} 5^\circ, & \text{IF } (c_3 \text{ OR } c_4) \text{ AND NOT}(c_1 \text{ OR } c_2) \\ -5^\circ, & \text{IF } (c_1 \text{ OR } c_2) \text{ AND NOT}(c_3 \text{ OR } c_4) \end{cases} . \quad (18)$$

For the manipulation of the object's translation and rotation, the command U_x in (11) controls via rotor-tilting the forward-exerted force, which is responsible for putting the object in longitudinal motion and is driven by the Euclidian distance error $e_x = \sqrt{(x^r - x)^2 + (y^r - y)^2}$. The U_y (or $\tilde{U}_y$) command controls the orientation of longitudinal motion and is driven by the orientation error $e_y = \tan^{-1}(\frac{y^r - y}{x^r - x})$. Two separate PI (Proportional, Integral) output-feedback loops at $f_X = 5$ Hz are implemented, considered adequate for handling the slow object translation and rotation dynamics. The Integral term is implemented in the form of a nonlinear Rate-Varying Integrator (RVI) [18] for position control of stick-slip friction systems.

Additionally, certain control constraints are observed by the FME control scheme, such that the Subsection III-B modeling requirement for stable docking contact is ensured:

$$U_x \geq U_x^{\min} = 5^\circ \quad |U_y| \leq S(U_x) \quad |\tilde{U}_y| \leq \tilde{U}_y^{\max} = 7.5^\circ \ . \tag{19}$$

$U_x^{\min}$ is a collective rotor-tilt angle that generates a minimum contact-maintaining forward-force. $\tilde{U}_y^{\max}$ is a maximum differential rotor-tilt angle such that the modeling approximation $r_{1_x} = r_{2_x} = r_{1,2_x}$ is maintained. $S(U_x)$ is the revolute end-effector γ_m angle threshold, for which lateral stiction at the virtual contact point is maintained. This is experimentally derived as a function of the normal-applied force (and thus the rotor tilt command U_x).

C. Finite State Machine Supervisory Controller

The FSM Supervisory Controller performs the guard-based transition between the system modes and provides reference signals, as determined by the specific task objectives, to the appropriately switched controller. Its operation is summarized in Figure 6. It consists of the following operation-related states, where the logical variable PLANAR_HOVER : $\{\phi,\ \theta,\ \psi\} \simeq \{0,\ 0,\ \psi^{obj} - \gamma_m\}$ denotes the successful UAV regulation around the planar-contact, hovering-attitude pose:

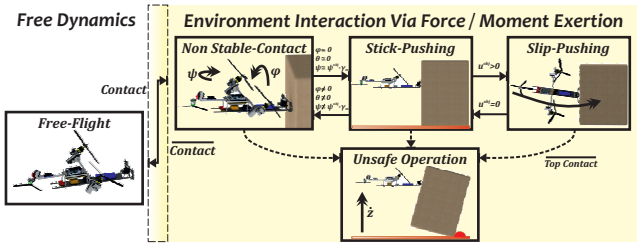

Fig. 6. Supervisory Controller Finite State Machine

a) The Free-Flight state, where no environment interaction takes place. The generated reference is either derived from the object reference docking-point $\mathbf{X_o}$ in order to initiate interaction, or is such that drives the UAV away from the object after completion of the manipulation objective. This state's active-condition guard-set is: ($\overline{c_1}$ AND $\overline{c_2}$ AND $\overline{c_3}$ AND $\overline{c_4}$).
b) The Non Stable-Contact state, where at least one tactile switch detects contact, and the UAV is not yet at PLANAR_HOVER. At this state, the minimum contact-maintaining U_x^{min} is applied. This state's active-condition guard-set is: (c_1 OR c_2 OR c_3 OR c_4) AND($\overline{\text{PLANAR\_HOVER}}$).
c) The Stick-Pushing state, where the UAV forward-exerted force is not sufficiently large to break the obstacle-to-ground interface stiction threshold, and thus $u^{obj} = 0$ from (5). The reference signal to the rotation P-RVI controller is disabled, as the object orientation is controlled only during longitudinal motion. The active-condition guard-set is: (c_1 AND c_2 AND c_3 AND c_4) AND (PLANAR_HOVER) AND ($u^{obj} = 0$).
d) The Slip-Pushing state, where sliding motion is in effect. The LTP-based position reference $\{x^r,\ y^r\}$ drives the translation and rotation P-RVI controllers, in order to achieve position setpoint manipulation of the object. The active-condition guard-set is: (c_1 AND c_2 AND c_3 AND c_4) AND (PLANAR_HOVER) AND ($u^{obj} > 0$).
e) The Unsafe-Operation state. A characteristic case is the detection of an improper docking point: as the object mass structure is unknown, it is possible that r_z^{obj} is such that a moment capable of tipping the object over is generated, as intuitively visualized in Figure 6. Such an active-condition guard-set would be: (c_2 OR c_4) AND ($\overline{c_1}$ AND $\overline{c_3}$) AND ($\dot{z} > 0$), reflecting the loss of contact on the end-effector top and the altitude rise.

V. EXPERIMENTAL STUDIES

For the experimental validation of the proposed approach an object of $m^{obj} \simeq 4.34$ kg was utilized. A forward-pushing force up to $F_x \simeq 22$ N was successfully exerted from the tiltrotor UAV in order to overcome stiction and manipulate the obstacle. It is noted that for this sizing a lift-and-carry strategy would be impossible, as the total rotor thrust margin is insufficient to support the combined UAV-and-object mass. However, the stiction force threshold is significantly lower and lies within the platform's capabilities. The accompanying video sequence demonstrates indicative respective results.

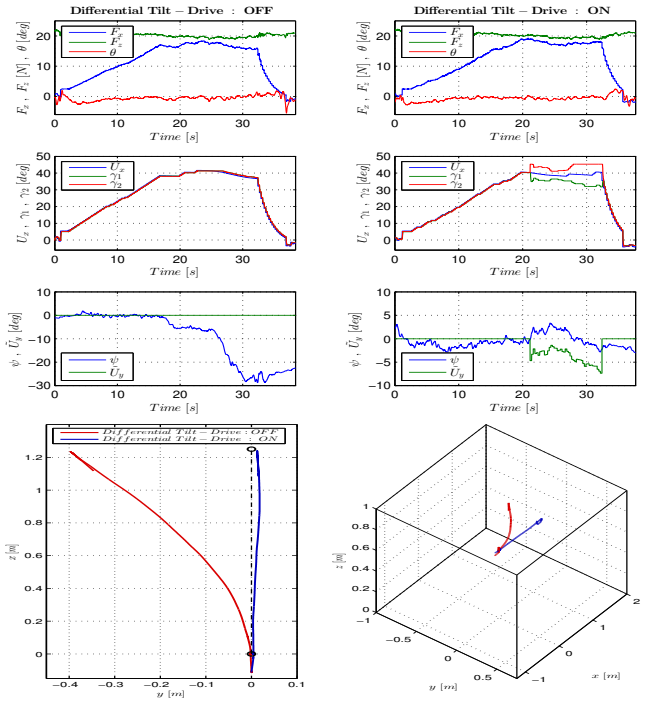

Fig. 7. Straight Setpoint Manipulation

For each experimental study the following results are provided: The top subfigures present the longitudinal-F_x and vertical-F_z forces generated by the UAV, and the pitch angle θ, indicating the effective decoupling of the UAV attitude and altitude throughout the sequence. The middle subfigures depict the main rotor tilt angles $\{\gamma_1,\ \gamma_2\}$ and the collective forward-tilt command U_x, while the third subfigures present the object estimated orientation-ψ and the rotating-moment command $\tilde{U}_y$ or U_y, according to the utilized control authority. Finally, 3D-plots visualize the resulting trajectories.

In Figure 7 straight setpoint manipulation is presented. With the $\tilde{U}_y$ differential-drive rotating-moment control authority disabled a straight trajectory cannot be ensured, as numerous uncertain parameters (object-COM position, ground texture) are crucial to the evolution of a non-ideal conditions experiment. In the first sequence it is noteworthy that the obstacle encounters higher-friction areas (near $t \simeq 20$ s and $t \simeq 22.5$ s where the U_x command is increased), with no significant disturbance induced on the hovering attitude pose.

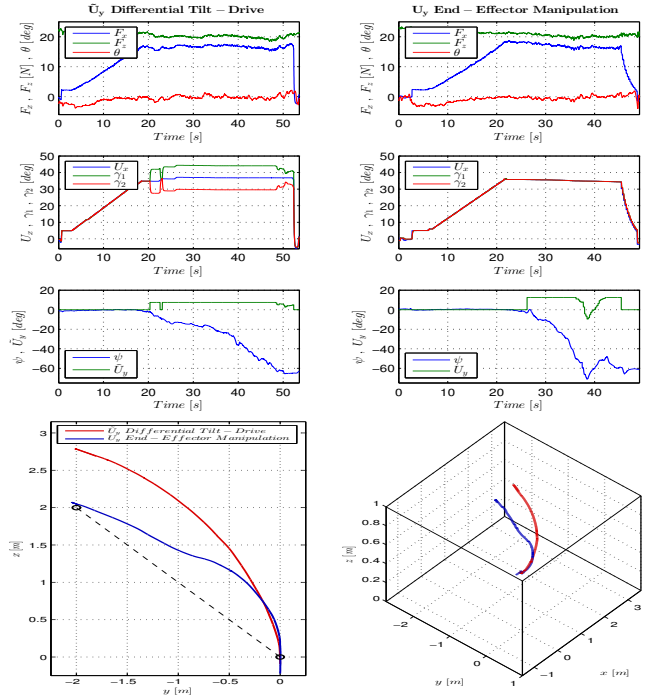

Fig. 8. Diagonal Setpoint Manipulation

In Figure 8 diagonal setpoint manipulation is presented, employing the $\tilde{U}_y$ differential-drive and the U_y end-effector manipulation principles. In these sequences, the Supervisory FSM controller maintains the reference signal until the setpoint y^r-coordinate has been reached. This provides the intuitive visualization of the effectiveness of each principle: The differential-drive moment control authority is insufficient for larger required moments, which in the object setpoint manipulation case-study appears as a large x^r overshoot.

The utility of direct thrust-vectoring as a technical asset in applications that require the exertion of large forces is noteworthy. The UAV manipulates its rotor-tilting authority up to $\gamma_x \simeq 45°$. At the same time, contrary to an underactuated system, it successfully remains near the hovering attitude pose where operational safety lies at maximum.

VI. CONCLUSIONS

An innovative implementation for the direct thrust-vectoring actuation authority of tiltrotor UAV types was presented. Rotor-tilting was employed in order to exert a large force in the longitudinal direction, while the retained attitude control authority ensured stable regulation near the hovering pose. Additionally, two methodologies were developed in order to enact a rotating moment, relying either on differential rotor tilting, or a separate active end-effector. This strategy's increased efficiency, in terms of effectiveness-versus-operational safety, was analyzed in a dedicated section. Finally, the proposed approach was experimentally validated on a mockup scenario, where an obstacle of twice the mass of the aerial platform was successfully manipulated via docked maneuvering while pushing.

REFERENCES

[1] K. Alexis, G. Nikolakopoulos, and A. Tzes, "Model predictive quadrotor control: attitude, altitude and position experimental studies," *Control Theory Applications, IET*, vol. 6, no. 12, pp. 1812–1827, 2012.

[2] A. Lussier-Desbiens, A. T. Asbeck, and M. R. Cutkosky, "Landing, perching and taking off from vertical surfaces," *IJRR*, vol. 30, no. 3, pp. 335–370, 2011.

[3] D. Mellingerm, Q. Lindsey, M. Shomin, and V. Kumar, "Design, modeling, estimation and control for aerial grasping and manipulation," in *Intelligent Robots and Systems (IROS), 2011 IEEE/RSJ International Conference on*, 2011, pp. 2668–2673.

[4] T. Justin, P. Joe, S. Koushil, and K. Vijay, "Avian-inspired grasping for quadrotor micro uavs," in *IDETC/CIE*. ASME, 2013.

[5] P. Pounds, D. Bersak, and A. Dollar, "Grasping from the air: Hovering capture and load stability," in *2011 International Conference on Robotics and Automation (ICRA)*, 2011.

[6] K. Kondak, K. Krieger, A. Albu-Schaeffer, M. Schwarzbach, M. Laiacker, I. Maza, A. Rodriguez-Castano, and A. Ollero, "Closed-loop behavior of an autonomous helicopter equipped with a robotic arm for aerial manipulation tasks," *International Journal of Advanced Robotic Systems*, vol. 10, no. 145, 2013.

[7] D. Mellinger, M. Shomin, N. Michael, and V. Kumar, "Cooperative grasping and transport using multiple quadrotors," in *Distributed Autonomous Robotic Systems*, ser. Springer Tracts in Advanced Robotics. Springer Berlin Heidelberg, 2013, vol. 83, pp. 545–558.

[8] L. R. M. Manubens, D. Devaurs, and J. Cortes, "Motion planning for 6d manipulation with aerial towedcable systems," in *Robotics Science and Systems Conference (RSS)*, Berlin, Germany, June 2013.

[9] M. Orsag, C. Korpela, and P. Oh, "Modeling and control of mm-uav: Mobile manipulating unmanned aerial vehicle," *Journal of Intelligent & Robotic Systems*, vol. 69, no. 1-4, pp. 227–240, 2013.

[10] K. Alexis, C. Huerzeler, and R. Siegwart, "Hybrid modeling and control of a coaxial unmanned rotorcraft interacting with its environment through contact," in *2013 International Conference on Robotics and Automation (ICRA)*, Karlsruhe, Germany, May 2013, pp. 5397–5404.

[11] B. L. Marconi, R. Naldi, and L. Gentili, "Modelling and control of a flying robot interacting with the environment," *Automatica*, vol. 47, pp. 2571–2583, 2011.

[12] C. Papachristos, K. Alexis, and A. Tzes, "Model predictive hovering-translation control of an unmanned tri-tiltrotor," in *2013 International Conference on Robotics and Automation (ICRA)*, Karlsruhe, Germany, May 2013, pp. 5404–5412.

[13] C. Papachristos, and K. Alexis, and A. Tzes, "Design and experimental attitude control of an unmanned tilt–rotor aerial vehicle," in *15th International Conference on Advanced Robotics*, Tallin, Estonia, 2011.

[14] C. Papachristos, K. Alexis, and A. Tzes, "Towards a high–end unmanned tri–tiltrotor: Design, modeling and hover control," in *Mediterranean Conference on Control Automation (MED)*, 2012, pp. 1579–1584.

[15] C. Papachristos and A. Tzes, "Large object pushing via a direct longitudinally-actuated unmanned tri-tiltrotor," in *Mediterranean Conference on Control Automation (MED), 2013*, pp. 173 –178.

[16] K. J. Astrom, "Control of systems with friction," in *Proceedings of the Fourth International Conference on Motion and Vibration Control*, 1998, pp. 25–32.

[17] S. B. Manohar, "Controlled manipulation using autonomous aerial systems," *Thesis (Ph. D.)–Massachusetts Institute of Technology, Dept. of Mechanical Engineering*, 2013.

[18] P. Tataryn, N. Sepehri, and D. Strong, "Experimental comparison of some compensation techniques for the control of manipulators with stick-slip friction," *Control Engineering Practice*, vol. 4, no. 9, pp. 1209 – 1219, 1996.